

# Two Missing Components for Solid Media Transmission: Amplifiers and Manifolds

Li Huang<sup>1</sup>, Xin Liu<sup>2</sup>, Nikolaos V. Tsekos<sup>2</sup>, Aaron T. Becker<sup>1</sup>

**Abstract**—Solid Media Transmission (SMT) is a new technology for transmitting robot actuation. SMT is similar to pneumatic or hydraulic transmissions, but uses solid balls and spacers rather than fluids to transmit force and displacement. SMT has been developed recently as a promising solution for specialized robot applications, including the challenges of confined space and strong magnetic field in Magnetic Resonance (MRI) scanners. Until now, SMT has lacked two capabilities compared to hydraulic and pneumatic devices: (1) manifolds, which can balance force among multiple inputs, and (2) amplifiers, which enable displacement scaling by trading force for displacement resolution. This paper introduces an SMT implementation for each of these missing components, provides scalable designs, parametric optimizations, hardware verifications, and ends with suggestions for future work.

## I. INTRODUCTION

A hydraulic transmission uses pressurized fluid to transmit force through small, flexible hoses. As illustrated in Fig. 1, hydraulic systems can perform force multiplication by modifying the effective ratio of cylinder area of the input and output cylinders. Moreover, multiple outputs can be connected to the same output through a hydraulic manifold for load balancing.

Hydraulics are useful in many areas of robotics, but have limitations for some specialized applications, such as environments where leakage is unacceptable such as clean rooms or surgery wards, temperature extremes including space, or large pressure variations such as undersea robotics. A new technology that attempts to combine the flexibility and ease of routing inherent to hydraulics without the need of pressurized fluid uses solid spheres to transmit force along flexible hoses. This solid media transmission (SMT) technology was first developed for use in magnetic resonance scanners [2].

## II. RELATED WORK

Magnetic resonance imaging (MRI) was applied to clinical diagnosis and treatment worldwide two decades after it was invented in early 1970's. Real-time MRI can produce high-quality images with in-plane resolution of 1 to 2 mm with only 20 to 30 ms processing time. This feature facilitates fast development of MRI-guide, robotic, minimally invasive intervention. Aided by real-time feedback of MRI, many robotic manipulators and platforms were proposed to perform

<sup>1</sup>L. Huang and A. Becker are with the Department of Electrical and Computer Engineering, University of Houston, Houston, TX 77004, USA {lhuang21, aabecker}@uh.edu

<sup>2</sup>X. Liu and N. Tsekos are with the Department of Computer Science, University of Houston, Houston, TX 77004, USA xliu43@uh.edu, nvtsekos@central.uh.edu

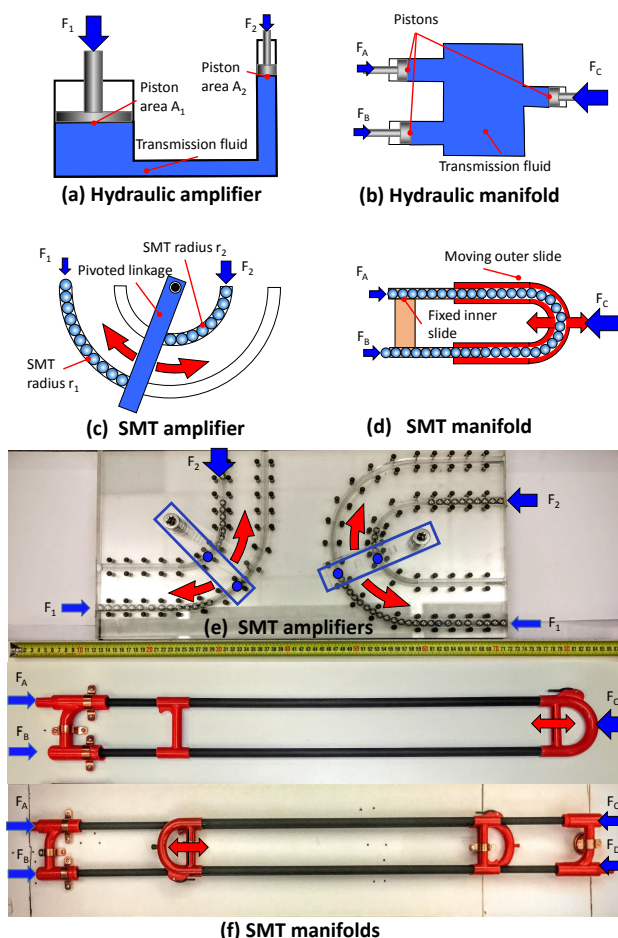


Fig. 1. Solid media transmissions are similar to hydraulic transmissions. This paper introduces amplifiers for precise displacement control based on a lever mechanism. And multiple-port manifolds enable balancing SMT actuation forces among multiple inputs. See video at [1].

safe and precise surgical procedure in tumor ablation and targeted biopsy. Larson B. T. et al. developed a robotic stereotactic device powered by ultrasonic motors and telescoping shafts to conduct MRI-guided probe insertion in the breast with prescribed trajectory and desired insertion depth [3]. A team led by Fischer G. S. used a pneumatic-actuated manipulator towards prostate biopsy under the guidance of MRI, achieving a positioning error of 0.94 mm RMS with multiple movements of the robotic system [4]. Integrated into imaging modality, real-time MRI was employed by Navkar N. V. et al. to provide visualization guidance of surgical access path planning, assisting human-in-the-loop operation

in beating heart intervention [5].

MRI guidance can significantly benefit robotic-assisted surgical operation, but also brings materials and transmission mechanism challenges. An MRI room is under high strength magnetic fields typically at 1.5 T to 3.0 T, exerting forces on any ferromagnetic equipment close to the MRI scanner. This force requires robotic transmission systems composed of non-magnetic materials. Hydraulic and pneumatic actuation have been widely investigated, as they are naturally electromagnetic compatible [6] [7]. However, physical constraints of the compact MRI bore limit practical applications of hydraulic transmission, which usually requires large space and is accompanied with risk of liquid leakage. Meanwhile, reliability may restrain clinical operations of pneumatic systems because of nonlinear dynamics, less robustness against force disturbances, and sensitivity to temperature changes. Recently, a novel solid media transmission (SMT) mechanism demonstrated a promising potential for clinical applications. Similar to hydraulic actuation, SMT tubes are instead loaded with solid sphere-bushing pairs. SMT is leak-free, compatible with 3D printing robots, and the transmission is flexible, enabling easy rerouting.

Hydraulic transmissions have the ability to tradeoff stroke length for force amplification by varying piston diameters, and can balance force between multiple inputs by sharing a common manifold. Compared to hydraulic transmissions, the SMT prototype only allowed single channel operation, and the displacement resolution was limited by the stepper motor. This paper presents solid media amplifiers and manifolds for SMT. These two improvements make SMT functionally comparable to applications of hydraulic and pneumatic transmissions. SMT amplifiers enable refined displacement resolution of the end effector, as shown in Fig. 1. A hydraulic manifold, also in Fig. 1, regulates in-tube media and directs the fluid into different openings. Inspired by the telescoping structure of a tenor trombone, the SMT manifold prototype was designed to balance multiple output forces of actuation.

Robot-assisted minimal invasive intervention requires demanding accuracy in SMT platform localization and needle placement. Equipped with amplifiers, SMT is capable of scaling down large translatory motion to precise movements, where the amplification ratio indicates the resolution improvement, and vice versa. Manifolds provide the ability to passively balance forces, useful for rerouting power and for tasks such as multi-finger gripping. Manifolds could provide adaptive and versatile structures for different MRI room setups.

### III. THEORY AND DESIGN

Force transmission and displacement control are key capabilities for robotic systems. Therefore, this paper introduces amplifiers and manifolds for SMT, aimed at displacement scaling and flexible actuation setup. These transmission designs are suitable for 3D printing, and hence can be disseminated widely to clinics and sites remote from main production locations.

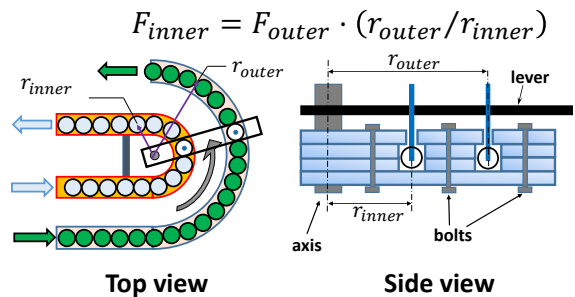


Fig. 2. An SMT amplifier with force amplification ratio  $a = r_{outer}/r_{inner}$ . As the outer tube is actuated, the lever passes the force and motion to the inner solid media and produces displacement and force scaling. Actuation forces applied from the inner tube to the outer tube give the amplification  $a^{-1}$ .

#### A. Design of Manifolds and Amplifiers

The design of amplifiers and manifolds is of special importance. When used for MRI, the SMT workspace is confined in the MRI scanner room and must be remotely controlled via a long transmission line. This poses particular design challenges: (1) how to operate manipulators in this limited space; (2) how to increase reliability and efficiency with the new transmission method.

1) *Amplifiers*: MRI-guided robotic surgery requires precise needle placement. It may require more precision than what is possible by an actuator powered remotely through a long SMT line. Fig. 2 shows a mechanical amplifier employed to achieve fine displacement control, where two channels are coupled with a lever. When spheres move  $s$  distance in the outer tube, the lever produces a resultant  $\frac{1}{a}s$  movement of solid media in the inner tube, where  $a$  denotes the amplification ratio. This shows a way to improve displacement resolution. Moreover, inverse motion (inner channel actuation) produces faster adjustment for SMT, as outer channel spheres travel  $a$  times farther than inner channel media.

2) *Manifolds*: The manifold mechanism was inspired by a musical instrument, the tenor trombone in Fig. 3. A trombone has a telescoping slide mechanism that varies the length of the instrument to change the pitch. The manifold balances forces among multiple ports. This figure shows a manifold of two components, a moving U-shaped outer tube, and a fixed inner tube that fits snugly into the outer tube. By combining tubes in parallel and serial, multi-port actuation can satisfy various transmission requirement.

#### B. Optimization of Parameters Towards Efficiency

In the prototype design, transmission reliability and efficiency can be improved considerably by optimizing the channel size, the turning angle, as well as the radius of a tubing bend. To give an explicit solution to this multivariable optimization problem, we present an analysis of the system dynamics in this section.

A design with zero-clearance would give ideal transmission efficiency because forces would be transmitted through the center of the SMT tube. However, manufacturing requires

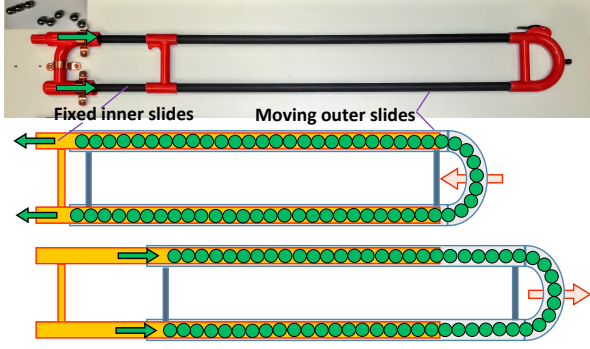


Fig. 3. A tenor trombone is used as the prototype of an SMT manifold. The manifold has a telescoping slide mechanism with two components: a pair of non-moving parallel tubes, and a U-shaped outer sheath. When actuated, the outer U-shaped tube slides along the inner component, following the motion of solid media loaded in the tube.

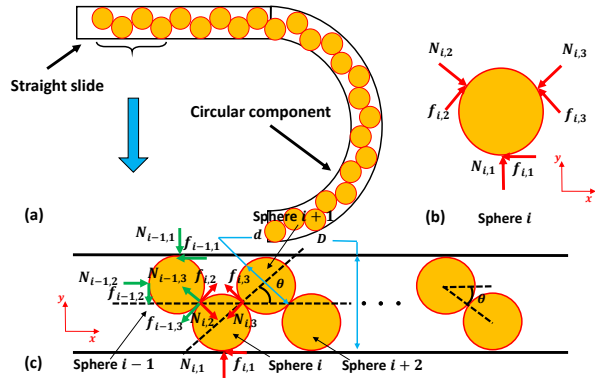


Fig. 4. (a) Spheres configuration in a tube depends on the size fit between them. A misalignment angle  $\theta$  determines the configuration of spheres in the SMT tube. (b) & (c) Considering a four-sphere unit, we observe that force distribution is similar for each unit because of their symmetric configuration.

clearances due to part tolerances. Therefore, it is reasonable to assume a minimal space configuration of solid media (spheres) in tubes as drawn in Fig. 4, and see math model at [8]. Without loss of generality, the following discussion of normal forces and friction considers four spheres as a unit where the balls are packed in an alternating configuration. Early experiments showed that spheres stay relatively static to each other as a result of large friction between steel surfaces. In most cases, sliding motion (rather than rolling) was observed between spheres and the tube wall.

For continuous contact of solid media in tubes, each unit shares similar dynamics. A general unit configuration is shown in Fig. 4. We name each element in a four-sphere system as  $i-1, i, i+1, i+2$  of Fig. 4b, with subscripts  $k \in \{1, 2, 3\}$ ,  $k=1$  as the reaction force against the wall,  $k=2, 3$  as forces between spheres. Taking sphere  $i$  as an example the force balance equations are

$$\sum F_x = 0, \sum F_y = 0, \sum \tau_o = 0, \quad (1)$$

where  $\tau_o$  stands for torques about the center  $o$  of sphere  $i$ .

Hence,

$$\begin{aligned} -f_{i,1} + N_{i,2} \cos \theta + f_{i,2} \sin \theta - N_{i,3} \cos \theta - f_{i,3} \sin \theta &= 0 \\ N_{i,1} - N_{i,2} \sin \theta + f_{i,2} \cos \theta - N_{i,3} \sin \theta + f_{i,3} \cos \theta &= 0 \\ f_{i,1}r + f_{i,2}r - f_{i,3}r &= 0 \end{aligned} \quad (2)$$

Here  $\theta$  stands for misalignment of spheres in a channel,  $r = \frac{d}{2}$  is the radius of a sphere, while  $N_{i,k}$  and  $f_{i,k}$  denote normal force  $k$  and friction  $k$  acting on sphere  $i$ , respectively.

$$\theta = \arcsin \frac{D-d}{d} \quad (3)$$

Note that  $\theta$  describes the angle between the  $x$ -axis and the line connecting centers of two spheres in contact.  $\theta$  increases as misalignment  $(D-d)$  accumulates. This implies a perfect alignment can be represented by  $\theta = 0$ , namely, an appropriate fitting of spheres in a tube.  $N_{i,2}$  and  $f_{i,2}$  are reaction forces from the left neighbor, and hence can be obtained by iteration. Then there are four unknown variables  $N_{i,1}, f_{i,1}, N_{i,3}, f_{i,3}$  in three equations above. So we use the fact that balls slide in tubes, and the following relation holds,

$$f_{i,1} = \mu N_{i,1} \quad (4)$$

with  $\mu$  the coefficient of dynamic friction between a ball and the wall. Writing these equations in matrix forms gives

$$Ax_i = Bx_{i-1} \quad (5)$$

$$x_i = A^{-1}Bx_{i-1} \quad (6)$$

with

$$x_{i-1} = [N_{i-1,1} \quad N_{i-1,3} \quad f_{i-1,3}]^T \quad (7)$$

$$= [N_{i-1,1} \quad N_{i,2} \quad f_{i,2}]^T \quad (8)$$

$$x_i = [N_{i,1} \quad N_{i,3} \quad f_{i,3}]^T \quad (9)$$

$$A = \begin{bmatrix} \mu & \cos \theta & \sin \theta \\ 1 & -\sin \theta & \cos \theta \\ -\mu & 0 & 1 \end{bmatrix} \quad (10)$$

$$B = \begin{bmatrix} 0 & \cos \theta & \sin \theta \\ 0 & \sin \theta & -\cos \theta \\ 0 & 0 & 1 \end{bmatrix} \quad (11)$$

And by iteration, force distribution is available at any location. The contours in Fig. 5 offer a direct view of normal force changes. Given an input force of 20 N along the channel, the force magnitude drops noticeably along a tubing bend. This implies that the turning angle is essential in parametric optimization. The spheres' configuration within a tubing bend in Fig 4, however, does not occur in our amplifiers due to the slots cut through the top and bottom layers to connect the lever arm. Hence, another configuration was applied in simulation, as Fig. 5 depicts.

Next, we investigate the influence of the radius  $R$  and the turning angle  $\alpha$  of a tubing bend, and the ratio  $\epsilon$  of sphere

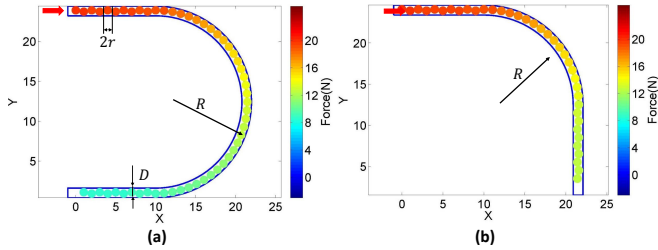


Fig. 5. Normal forces distribution between spheres in tubes for a  $180^\circ$  and a  $90^\circ$  turning angle with  $\epsilon = 0.970$  of sphere diameter to tube width, and  $\mu = 0.22$  of friction coefficient between wall and spheres. Given a 20 N input force, the output force in case (a) is 8 N output, and case (b) 12 N. This comparison shows a marked loss in force efficiency along the tubing bend. It implies that large turning angles are undesirable for force transmission.

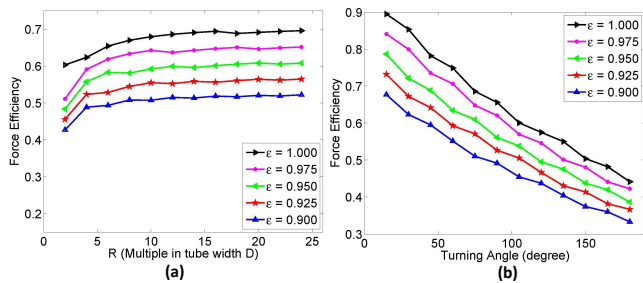


Fig. 6. (a) Relation between force transmission efficiency against radius ( $R$ ) of the tubing bend with  $\mu = 0.22$ . A larger radius yields increased efficiency. Efficiency plateaus as the radius  $R \geq 10D$ . (b) Force efficiency as a function of turning angle. Efficiency drops linearly with increasing turning angle. In both cases, efficiency drops as the ratio  $\epsilon$  of sphere diameter to tube width decreases below unity.

diameter to channel width to give an optimal design. Fig. 6 presents force efficiency of two simulations. Fig. 6a suggests a  $90^\circ$  tubing bend, where a larger radius bend  $R$  (in multiple of tube width  $D$ ) leads to a higher transmission efficiency. Tighter fits of spheres with the tube, specifically  $\epsilon = \frac{2r}{D} \rightarrow 1$ , improves efficiency. If the radius  $R \leq 5D$ , unfavorable transmission failure may happen. Fig. 6b describes outcomes using different turning angles, and ratios of sphere diameter to tube width. SMT efficiency improves with smaller turning angles. Substituting a  $20^\circ$  for  $180^\circ$  tubing bend with  $\epsilon = 0.975$  increases efficiency by 40%.

Typically, needle placement of SMT requires a 0 to 100 mm range of solid media movement. This indicates a range of 0 to  $100a$  mm displacement ( $L$ ) for spheres in the outer channel, with  $a$  the amplification ratio. This length constrains the radius of the tubing bend  $R$  according to  $L = R\alpha$ , where  $\alpha$  is the turning angle. Considering the compact space of a MRI room, the radius  $R = 10D$  is chosen, with the tube width  $D=11.2$  mm. It follows that an optimal turning angle is  $\alpha = \frac{L}{R} = \frac{100a}{112} = 0.893a$ . Assuming that the targeted amplification ratio is  $a = 2$ , an appropriate design of the turning angle is  $\approx 1.786$  radians, or  $102^\circ$ . Were better transmission required,  $\alpha$  should decrease and the radius  $R$  will increase accordingly.

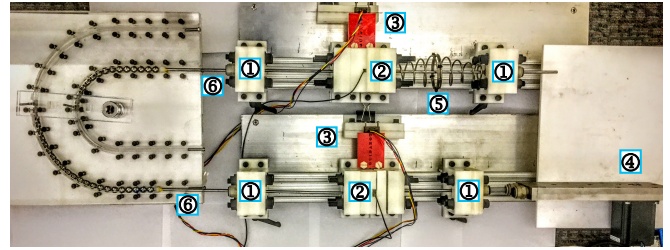


Fig. 7. The experiment setup for the amplifier transmits force from a motor, through a sensor suite, to one raceway of the amplifier and out the other raceway, through a second sensor suite and terminates on a compression spring. The actuation slide rail has a stepper motor (4), while the force-hold slide rail terminates in two conical compression springs (5). Each slide rail has two fixed cubes (1) at each end, and two moving cubes (2) in the middle. Next to the moving cubes lies an optical encoder (3), and force sensors are embedded in the cubes. Steel rods (6) connect the test object to the stepper motor and the springs. The rod passes through each cube on the rail.

#### IV. EXPERIMENTS AND RESULTS

To evaluate SMT transmission efficiency with manifolds and amplifiers, we followed the experiment procedure of Liu et al. [2]. The experiment setup is presented in Fig. 7, which consists of three components: actuation slide rail, force-hold slide rail, and the test object. Force and displacement can be detected via force sensors and optical encoders. The passive force-hold rail uses two conical compression springs to generate a holding force while the actuation slide rail uses a stepper motor.

Given a PWM control signal, the stepper motor gear drives the steel rod back and forth horizontally. For an NEMA-24Y508 motor, the output is provided by a mechanical transmission made of a rack and pinion with a transmission ratio of 0.249 mm/motor-step or 89.78 mm/rev. In experiments, the actuation procedure proceeds at 0.5 Hz. A full operation includes a push and a retraction on solid media. For example, at time  $t_0$ , the motor rotates  $N$  steps clock-wise, and then holds its position. At time  $t = t_0 + 1$ , the motor releases, spins counter clock-wise for the same number of steps, and holds its position. This repeats for more than 25 rounds. The optical encoders and force sensors were recorded at a 1000 Hz sampling rate.

The goal of this experiment is to quantify the displacement resolution the amplifier can provide for solid media and to demonstrate the capability of manifolds for multi-port transmission with SMT. Different step sizes were chosen to test the range of effective transmission.

##### A. Hardware Design

Two amplifiers were built using four layers of laser cut acrylic. Each layer was made of 5.6 mm thick acrylic with 11.2 mm width passageways for 11.2 mm diameter steel spheres. The first amplifier has two tubing bends of  $180^\circ$ , where the inner bend has a 63.5 mm radius, and the outer bend has a 127 mm radius. The second amplifier uses the same pair of radii, but a  $90^\circ$  bend angle instead.

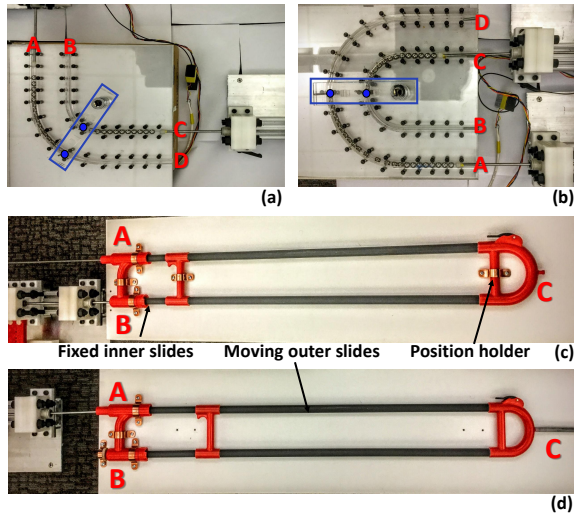


Fig. 8. (a) - (b) Two amplifiers prototype in Case 2 ( $A \rightarrow C$ ) and Case 3 ( $C \rightarrow A$ ). (c) - (d) The manifold prototype in Case 1 ( $A \rightarrow B$ ), Case 2 ( $A \rightarrow C$ ), and Case 3 ( $C \rightarrow A$ ).

The prototype test of a manifold employs a 700 mm long tenor trombone, with 12.2 mm inside diameter, and the distance between centerlines of the two parallel tubes is 85.7 mm. The manifold was loaded with steel spheres of 11.9 mm diameter.

### B. Characterizing Amplifier Performance

There are two goals of experiments on amplifiers. One is to verify the potential of displacement resolution improvement, and the other one to compare the minimal space configuration model in Section III with prototype test data.

90° and 180° amplifiers were used for the experiment, as shown in Fig. 8a and Fig. 8b. The first study examined the single channel transmission of SMT in both amplifiers. In Case 1 and Case 3, the stepper motor pushes spheres in the outer channel from port  $A$  and results in the spheres motion through port  $D$  in the 90° and the 180° amplifier, respectively. Case 2 demonstrates the inner channel transmission in the 90° amplifier, with port  $B$  as the input and port  $C$  as the output. Three cases presented in Fig. 9 were aimed at validating the minimal space configuration, with no amplification mechanism. All cases produced impressive displacement efficiency of over 90% independent of input, with reliable standard deviation no greater than 0.1. This rigid motion is a valuable property of SMT, and followed the minimal-space configuration suggested in Fig. 4, and hence proves the capability for accurate displacement control. Fig. 9b shows the experiment results of the force transmission ratio. When compared to simulations in Fig. 6, it reveals a strong consistency of radius and turning angle impact on force efficiency.

The next test examined the overall performance of amplifiers with a 90° and a 180° tubing bend. Case 1 ( $A \rightarrow D$ ) on both amplifiers presented the single channel results for comparison, with no amplification. Case 2 ( $A \rightarrow C$ ) explored

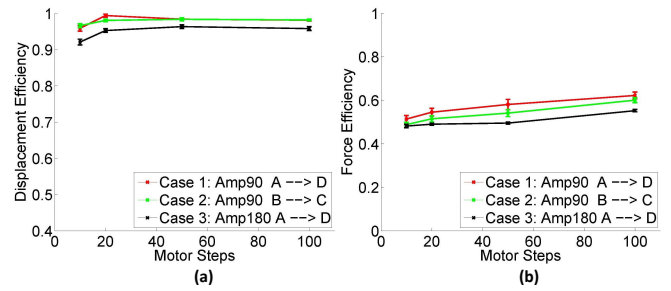


Fig. 9. Experiments on amplifier prototypes with 25 trials of each data point: (a) The displacement responses in single channel trials demonstrate the high reliability and efficiency of SMT. The relatively rigid motion benefits from the property of solid media, which is consistent with the minimal space configuration. (b) Force efficiency reveals details of SMT performance when design parameters change. The experiment data validate the effectiveness of simulation results in Fig. 6, and show significant influence of the turning angle and the radius upon force efficiency.

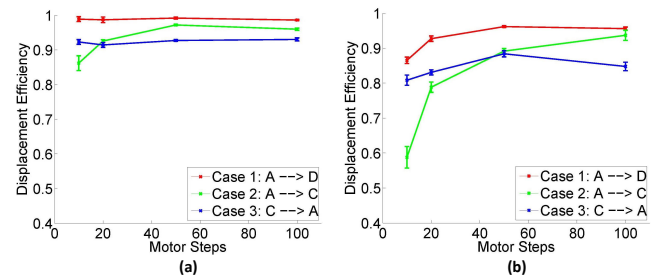


Fig. 10. Experiments on amplifier prototypes with 25 trials of each data point: (a) and (b) present the displacement efficiency of the 90° and the 180° amplifier, respectively. In general, the 90° amplifier has impressive displacement transmission ratio, where most data points achieve a mean efficiency of better than 90%. The performance of the 180° amplifier is comparable to the 90° case, with a slight drop in efficiency.

amplification effect in displacement, where spheres from outer channel transmit force and motion to the inner solid media via a lever part. Case 3 ( $C \rightarrow A$ ) was set to check an inverse movement where port  $C$  was made the actuation side. Fig. 10a and Fig. 10b show the displacement efficiency of the 90° and the 180° amplifier, respectively. All three cases provide convincing outcomes for transmission reliability with small standard deviation. In general, the 90° amplifier has a high displacement transmission ratio, where most data points achieve a mean efficiency of better than 90%. The performance of 180° amplifier is marginally comparable to the 90° case, despite of a slightly drop in efficiency. The amplification ratio is set as 1/2 in Case 2, and hence the 100% efficiency is based on expected transmission, namely, 1/2 of the input. The mean efficiency at 10 steps (2.24 mm displacement) is relatively imperfect for each amplifier, but note that the resultant expected output would be only 1.12 mm, which is demanding for the optical encoders (0.05 mm resolution) we use. The larger standard deviations at 10 steps in Case 2 also imply such outcomes might be caused by the limited resolution of the optical encoders.

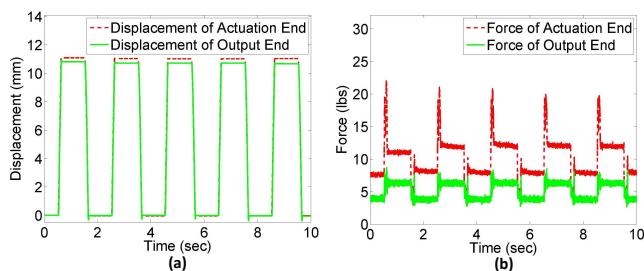


Fig. 11. Experiments on the 3-port manifold prototype. Force and displacement data from the first 10 seconds of Case 1 at 50 motor steps. (a) The displacement responses of the manifold track the input steps. (b) The spikes in force transmission at the beginning of each step mark a transition from large static friction to dynamic friction.

### C. Characterizing Manifold Performance

The manifold was attached to a wooden board to conduct three-way transmission experiments. The straight inner tubes were bolted to the board, and the U-shaped slide was allowed to move freely. A similar experiment procedure was followed as with the amplifiers to explore the manifold mechanism. The mechanism of this simple manifold is explained in Section III. The inlets to the straight tubes are labelled *A* and *B*, and forces applied to the U-shaped tube are labelled *C*. As shown in Fig. 8, in Case 1 ( $A \rightarrow B$ ), port *C* was locked by a position holder, and steel spheres were pushed through port *A* and port *B*. Therefore some spheres pass through a  $180^\circ$  movement. In Case 2 ( $A \rightarrow C$ ), port *B* was locked, and thus the actuation via port *A* led to motion of port *C*, namely, both spheres and the U-shaped outer tube move. In Case 3 ( $C \rightarrow A$ ), an opposite movement to Case 2 was investigated with port *C* as the actuation input, and port *A* connected to a compression spring.

The manifold experiment studied SMT performance of straight channels and tubing bends. Fig. 11 shows the satisfactory repeatability and immediate responses of both displacement and force in the manifold. This figure documents the first 10 seconds of Case 1 at 50 motor steps. The spikes in force at the beginning of each step were caused by large static friction. Fig 12 gives an overall evaluation of the manifold performance for three cases. The displacement responses show outstanding mean efficiencies over 90%, with little standard deviations. Fig 12b presents force transmission ratio against motor steps. The three cases all have consistent behavior and an efficiency of over 50%, showing smooth transmission during the experiment.

## V. CONCLUSIONS

This paper introduced a scalable SMT implementation of amplifiers and manifolds. These components make SMT functionally comparable to hydraulic or pneumatic transmissions. The paper presented hardware implementations of SMT amplifiers and a manifold. Each component was verified in a series of experiments. The  $90^\circ$  amplifier and the manifold produce highly reliable and desirable displacement responses, with over 90% efficiency in most cases. Parametric optimization based on a minimal space configuration

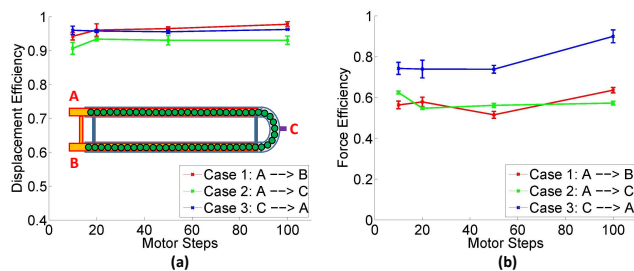


Fig. 12. Experiments on the 3-port manifold prototype. 25 trials were run for each datapoint, and summarized by the average and  $\pm$ one standard deviation. (a) The displacement responses show outstanding mean efficiencies over 90%, with little standard deviations. And (b) presents force transmission ratio against motor steps. Three cases all have consistent behavior, and efficiency of over 50% shows smooth transmission during the experiment.

has favorable results with experiments data, which can be further extended to direct design in SMT manifolds and amplifiers. There are many opportunities for future work. The amplifiers introduced in this paper have a limited stroke length. Building an infinite-length amplifier is a current challenge. The nature of friction along an SMT tube requires additional studies and theory.

## ACKNOWLEDGMENT

This material is based upon work supported by the National Science Foundation under Grant No. IIS-1553063 (ATB) and CNS-0932272 (NVT). Any opinions, findings, and conclusions or recommendations expressed in this material are those of the author(s) and do not necessarily reflect the views of the National Science Foundation.

## REFERENCES

- [1] L. Huang, "Solid media transmission (SMT) — manifolds and amplifiers," <https://youtu.be/Li6ewNC9Zxo>, accessed: 03-28-2016.
- [2] X. Liu, D. Biediger, R. Kopru, E. G. Christoforou, and N. V. Tsekos, "A new transmission mechanism for the actuation of manipulators for magnetic resonance imaging (MRI) guided interventions," pp. 673–678, 2016.
- [3] B. T. Larson, A. G. Erdman, N. V. Tsekos, E. Yacoub, P. V. Tsekos, and I. G. Koutlas, "Design of an MRI-compatible robotic stereotactic device for minimally invasive interventions in the breast," *Journal of Biomechanical Engineering*, vol. 126, no. 4, pp. 458–465, 2004.
- [4] G. S. Fischer, I. Iordachita, C. Csoma, J. Tokuda, S. P. DiMaio, C. M. Tempany, N. Hata, and G. Fichtinger, "Mri-compatible pneumatic robot for transperineal prostate needle placement," *Mechatronics, IEEE/ASME Transactions on*, vol. 13, no. 3, pp. 295–305, 2008.
- [5] N. V. Navkar, Z. Deng, D. J. Shah, K. E. Bekris, and N. V. Tsekos, "Visual and force-feedback guidance for robot-assisted interventions in the beating heart with real-time MRI," in *Robotics and Automation (ICRA), 2012 IEEE International Conference on*. IEEE, 2012, pp. 689–694.
- [6] S. Hao, A. Camilo, G. A. Cole, H. Nobuhiko, C. M. Tempany, and G. S. Fischer, "High-field MRI-compatible needle placement robot for prostate interventions," *Studies in health technology and informatics*, vol. 163, p. 623, 2011.
- [7] N. Yu, C. Hollnagel, A. Blickenstorfer, S. S. Kollias, and R. Riemer, "Comparison of MRI-compatible mechatronic systems with hydrodynamic and pneumatic actuation," *Mechatronics, IEEE/ASME Transactions on*, vol. 13, no. 3, pp. 268–277, 2008.
- [8] A. Becker and L. Huang, "Packing spheres into a thin cylinder," <http://demonstrations.wolfram.com/PackingSpheresIntoAThinCylinder/>, accessed: 06-30-2016.